Materials Today Bio 25 (2024) 100962

Contents lists available at ScienceDirect

Materials Today Bio

journal homepage: www.journals.elsevier.com/materials-today-bio

Injectable silk fibroin peptide nanofiber hydrogel composite scaffolds for cartilage regeneration

Deguang Wu [a], Jian Li [a], Chengxinqiao Wang [a], Zhiwen Su [a], Hao Su [a], Yan Chen [b,**], Bo Yu [a,*]

[a] Department of Orthopedic and Traumatology, Zhujiang Hospital, Southern Medical University, Guangzhou, 510282, China
[b] Ultrasound Medical Center, Zhujiang Hospital, Southern Medical University, Guangzhou, 510282, China

ARTICLE INFO

Keywords:
Self-assembling peptide
Silk fibroin
Cartilage regeneration
Injectable
TGF-β1

ABSTRACT

Transforming growth factor-β1 (TGF-β1) is essential for cartilage regeneration, but its susceptibility to enzymatic denaturation and high cost limit its application. Herein, we report Ac-LIANAKGFEFEFKFK-NH_2 (LKP), a self-assembled peptide nanofiber hydrogel that can mimic the function of TGF-β1. The LKP hydrogel is simple to synthesize, and *in vitro* experiments confirmed its good biocompatibility and cartilage-promoting ability. However, LKP hydrogels suffer from poor mechanical properties and are prone to fragmentation; therefore, we prepared a series of injectable hydrogel composite scaffolds (SF-GMA/LKP) by combining LKP with glycidyl methacrylate (GMA)-modified silk fibroin (SF). SF-GMA/LKP composite scaffolds instantaneously induced *in-situ* filling of cartilage defects and, at the same time, relied on the interaction between LKP and SF-GMA interaction to prolong the duration of action of LKP. The SF-GMA/LKP10 and SF-GMA/LKP20 composite scaffolds had the best effect on neocartilage and subchondral bone reconstruction. This composite hydrogel scaffold can be used for high-quality cartilage repair.

1. Introduction

Due to the lack of lymphatic circulation and direct blood supply in the knee joint cavity, the nutritional supply of articular cartilage is dependent mainly on joint fluid, so the self-repairing ability of articular cartilage is very limited after injury [1–3]. Continued progression leads to progressive destruction of articular cartilage and eventually to osteoarthritis. TGF-β1 is an important regulator of cartilage regeneration [4]. TGF-β1 activates SMAD signalling pathways by recruiting mesenchymal stem cells to the joint cavity, thereby inducing cartilage formation and enhancing the synthesis of proteoglycans, cartilage oligomeric proteins, and type II collagen [5,6]. However, due to a lack of blood supply, TGF-β1 cannot be recruited to the joint cavity through the blood [7], thus affecting articular cartilage regeneration. Unfortunately, direct loading of exogenous TGF-β1 is prone to sudden release, resulting in toxicity, and is susceptible to enzymatic denaturation, thus limiting its clinical application [8].

Functional motifs are usually derived from the amino acid sequences of certain growth factors. These functional motifs can partially or completely simulate the physiological function of the corresponding growth factors [9]. In previous studies, LIANAK, a TGF-β1 mimetic peptide, was synthesized simply and inexpensively and could promote angiogenesis, skin repair, and cartilage regeneration by exerting TGF-β1-like effects, making it an ideal alternative to TGF-β1 [10]. However, the application of LIANAK alone still results in rapid release and requires a suitable delivery system is needed to maintain the concentration required for cartilage regeneration. Based on this, we used a self-assembly sequence to covalently bind with LIANAK to form a hydrogel (LIANAKGFEFEFKFK, named LKP) to accomplish the function of delivering mimetic peptide. Pure self-assembling peptide hydrogels have low mechanical strength and a fast degradation rate. Therefore, a novel drug delivery system is needed to improve the efficacy of cartilage repair.

Silk fibroin (SF) is widely used in medical fields such as vascular stents, medical cosmetology, and wound dressing, and so on and has good biocompatibility [11–15]. SF is slightly soluble in water due to its high degree of crystallization [16,17]. This hydrophobic property makes it difficult to obtain a uniform structure when the material is combined with hydrophilic systems such as hydrogels. To improve the solubility of SF, salt dissolution and dialysis are often used to obtain SF, which is

* Corresponding author.
** Corresponding author.
E-mail addresses: smu_chen@163.com (Y. Chen), gzyubo@163.com (B. Yu).

https://doi.org/10.1016/j.mtbio.2024.100962
Received 26 October 2023; Received in revised form 25 December 2023; Accepted 15 January 2024
Available online 22 January 2024

subsequently prepared with the corresponding composite system [18,19]. The preparation of SF solution prepared by this method is complex, has poor stability, and is often prone to spontaneous gelation, which limits its use. The addition of glycidyl methacrylate (GMA) groups to SF by grafting increases the solubility of SF and can be used for photopolymerization to form hydrogels [20,21]. Moreover, some studies have confirmed that the addition of peptides can change the conformation of SF, creating composite hydrogels with variable mechanical properties [22,23]. However, peptide doping to change the SF conformation to form a stable hydrogel often takes 5–30 min, which is not favourable for clinical application. Therefore, we envisioned that the peptide would be doped into SF-GMA instead of SF to rapidly form a stable hydrogel via photopolymerization, while the peptide would further slowly change the SF-GMA conformation to form a more stable composite hydrogel with better mechanical properties.

In summary, we designed an LKP self-assembled peptide nanofiber hydrogel that mimics the function of TGF-β1 and validated it *in vitro*. Moreover, we utilized the principle that peptides can change the SF conformation, and for the first time, we doped the LKP peptide into SF-GMA and prepared an injectable peptide nanofiber hydrogel composite scaffold (named SF-GMA/LKP) with excellent physical and biological properties. The biosafety and efficacy of SF-GMA/LKP in promoting cartilage repair were evaluated *in vitro* and *in vivo*.

2. Materials and methods

2.1. Materials

Ac-LIANAKGFEFEFKFK-NH_2 (LKP) and Ac-FEFEFKFK-NH_2 (EKP) were synthesized by solid-phase synthesis at Wuhan Xinghao Pharmaceutical Co. (Wuhan, China). Mulberry cocoons were purchased from Beijing Yihong Guangjie Biotechnology Co., Ltd., and lithium phenyl (2,4,6-trimethylbenzoyl) phosphate (LAP) was purchased from Shanghai Bide Pharmaceutical Technology Co., Ltd. (Shanghai, China). Lithium bromide (LiBr) and GMA were purchased from Shanghai Aladdin Biochemical Technology Co., Ltd. FBS and DMEM/F12 were purchased from Gibco (Grand Island, USA). All the experimental animals were obtained from the Guangdong Medical Laboratory Animal Center (Foshan, China).

2.2. Preparation of self-assembled polypeptide hydrogels and SF-GMA

Five milligrams of LKP and EKP peptide powders were accurately weighed, dissolved in 1 mL of Milli-Q water (Millipore, Germany), adjusted to pH 7.0–7.4 to obtain the corresponding peptide nanofiber hydrogels, and subsequently stored at 4 °C for spare use.

The preparation of SF-GMA was performed as described previously [21]. In brief, SF can be obtained by chopping mulberry cocoons (20 g), adding 1 L of 0.05 M Na_2CO_3, boiling at 100 °C for 30 min, rinsing, and drying with distilled water. Then, 20 g of SF was dissolved in 100 mL of 9.3 M LiBr solution at 60 °C for 1 h, 6 mL of GMA was added to continue the reaction for 6 h, and SF-GMA was obtained by dialysis and freeze-drying.

2.3. Preparation of injectable light-curable SF-GMA/LKP hydrogel scaffolds

SF-GMA/LKP hydrogel scaffolds were synthesized as follows. The photoinitiator LAP was added to a 10 % w/v SF-GMA solution at a concentration of 0.2 % w/v, four different bioinks were subsequently prepared with 5 mg/mL LKP peptide nanofiber hydrogels at a volume ratio of 100:0 (SF-GMA/LKP0), 95:5 (SF-GMA/LKP5), 90:10 (SF-GMA/LKP10), or 80:20 (SF-GMA/LKP20), and hydrogel scaffolds were formed under UV irradiation.

2.4. Characterization of peptide nanofiber hydrogels

2.4.1. Circular dichroism (CD)

LKP and EKP peptide nanofiber hydrogels (5 mg/mL) were diluted to 0.1 mg/mL with Milli-Q water. A 1 mm colorimetric plate was used in the CD spectrometer (BRIGHTTIME Chirascan, UK) to scan from 190 nm to 400 nm under the protection of nitrogen.

2.4.2. Fourier transform infrared spectroscopy (FTIR)

Freeze-dried samples of 5 mg/mL LKP and EKP peptide nanofiber hydrogels were placed in the FTIR (Nicolet-iS50, America) detection window and evaluated in the 1300-2000 cm^{-1} region.

2.4.3. Transmission electron microscopy (TEM)

LKP and EKP peptide nanofiber hydrogels (5 mg/mL) were diluted 40 times, added to a porous carbon mesh mounted on a copper mesh, dried, and imaged via TEM(JEM F200, Japan).

2.4.4. Scanning electron microscopy (SEM)

The 5 mg/mL LKP and EKP peptide nanofiber hydrogels were diluted five times and freeze-dried, and the samples were subsequently plated with gold to increase the electrical conductivity. The images were acquired via SEM (TESCAN, Czech Republic). The operating voltage was 5 kV.

2.4.5. Atomic force microscopy (AFM)

Briefly, 5 mg/mL LKP and EKP peptide nanofiber hydrogels were sonicated for 20 min and diluted 10-fold, after which the samples were deposited on the sample stage for 15 s. The samples were air-dried for image acquisition (Bruker, Germany).

2.5. Characterization of the SF and SF-GMA/LKP hydrogel scaffolds

2.5.1. FTIR

The freeze-dried SF-GMA and SF samples were placed in the FTIR detection window and evaluated in the 800–2500 cm^{-1} spectral region.

Four freeze-dried SF-GMA/LKP hydrogel samples were placed in the FTIR detection window and evaluated in the 1300-1800 cm^{-1} region.

2.5.2. SEM

Briefly, four SF-GMA/LKP specimens were freeze-dried and subjected to brittle fracturing with liquid nitrogen. Then, the samples were gold-plated, and images were captured via SEM.

A total of 5×10^5 rat BMSCs were seeded on four porous hydrogel scaffolds and then cultured in DMEM/F12 medium supplemented with 10 % FBS at 37 °C in a 5 % CO_2 incubator for one day. The scaffolds were fixed with 4 % paraformaldehyde for 30 min and dried at the critical point. The samples were plated with gold to increase the electrical conductivity, and images were acquired via SEM. The operating voltage was 5 kV.

2.6. Nuclear magnetic resonance spectroscopy (1H NMR)

1H NMR analysis of the molecular structure and degree of substitution of SF-GMA. The sample was placed in a 5 mm sample tube, D2O was added to fully dissolve the sample, and nuclear magnetic resonance (Bruker, Japan) was used to analyse the data.

2.6.1. Rheological analysis of SF-GMA/LKP

Four SF-GMA/LKP solutions were prepared according to the method in Section 2.3. The rheological properties of the four different bioinks were evaluated by a parallel plate rheometer (Malvern, UK) at 25 °C and 37 °C. The scanning range was 0.1–100 rad/s, the plate diameter was 40 mm, and the test gap was 0.5 mm.

2.6.2. Degradation and swelling of SF-GMA/LKP

To test degradation, 600 μL of each of the SF-GMA/LKP hydrogel scaffolds was soaked in 5 mL of PBS (PH 7.4, 37 °C) for predefined time intervals. The SF-GMA/LKP hydrogel scaffolds were freeze-dried and weighed. The hydrogel scaffolds were removed after soaking for 1, 4, 7, 14, 21, or 28 days and were weighed after freeze-drying.

The cell strainers were weighed correctly (W0). Five hundred microlitres of SF-GMA/LKP hydrogels were deposited on the cell strainers and weighed together (W1). Then, the cell strainers were placed in 5 mL of PBS, the SF-GMA/LKP hydrogels were swelled within a certain period, and both (W2) were correctly weighed after the filter paper absorbed surface moisture. Three samples per group were tested. The swelling ratio was calculated as follows:

$$\text{Swelling ratio}\ (100\%) = (W2 - W1)/(W1 - W0) \times 100\%$$

2.7. Biocompatibility of peptide nanofiber hydrogels and SF-GMA/LKP

The biocompatibility of the peptide nanofiber hydrogel and SF-GMA/LKP was evaluated by a cell counting kit-8 (CCK-8) and live-dead staining. In brief, 1 mL of peptide nanofiber hydrogel or SF-GMA/LKP hydrogel was placed in 49 mL of DMEM/F12 medium for 2 days, filtered and sterilized, and then cocultured with rat BMSCs on 48-well plates. After 1, 4, and 7 days of coculture, 200 μL of culture medium containing CCK-8 was added, the cells were incubated at 37 °C for 2 h in the dark, and the OD values at 450 nm were subsequently detected for enzyme calibration (Biotech, USA).

Accordingly, a live-dead staining kit (Beyotime, China) was used to evaluate the effect of the peptide nanofiber hydrogel and SF-GMA/LKP hydrogel on rat BMSCs. Briefly, the peptide nanofiber hydrogel or SF-GMA/LKP hydrogel and rat BMSCs were cocultured for 1, 4, or 7 days, after which 100 μL of living and dead staining working solution was added. After incubating for 10 min in the dark, the cells were observed under a Nikon high-content inverted fluorescence microscope (Nikon, Japan).

We used three-dimensional cultures to confirm the biosafety of the SF-GMA hydrogel. To create hydrogels, 3×10^5 BMSCs were combined with SF-GMA/LKP solutions and deposited on 14-mm round coverslips (Biosharp, China). UV irradiation was then applied for 10 s. After adding 2 mL of DMEM/F12 media for 1 day of coculture, 2 mL of live cell staining working solution was added to each 6-well plate with circular coverslips. A Nikon confocal microscope (Nikon, Japan) was used to capture images after 30 min of incubation in the dark.

2.8. Western blot (WB) and real-time PCR (RT–PCR)

Rat BMSCs were treated with peptide nanofiber hydrogels and SF-GMA/LKP hydrogels. For sample preservation, the loading buffer was supplemented with the total protein extracted from the three groups of cells, which were subsequently boiled at 100 °C. Protein samples of different molecular weights were separated via SDS–PAGE (Epizyme, China), then transferred to a nitrocellulose membranes and blocked with 5 % skim milk powder for 1 h. Primary antibodies against collagen type II (Col-II) (1:1000, 28459-1-AP,Proteintech, China) and recombinant sex determining region Y box protein 9 (Sox9) (1:1000, 67439-1-Ig, Proteintech, China) were used to specifically label the target proteins. The corresponding protein signals were then labelled with secondary antibodies and developed via chemiluminescence (UVITEC, UK) with an enhanced chemiluminescence ECL kit (SQ101, Epizyme, China). A semiquantitative analysis of the target proteins was performed using Nine Alliance software.

Total RNA was extracted from the samples and reverse transcribed using AG RNAex Pro Reagent (AG, China). The samples were assayed for gene expression using SYBR Premix EX Taq (TaKaRa, Japan). Chondrogenesis-related genes were quantified using the 2ˆ-ΔCT method.

2.9. Immunofluorescence staining

The peptide nanofiber hydrogel and SF-GMA/LKP hydrogel were cocultured with rat BMSCs for 2 days. BMSCs were then fixed with 4 % paraformaldehyde for 10 min, permeabilized with 0.2 % Triton for 10 min, and incubated in 1 % BSA (PBST + 22.5 mg/mL glycine) for 1 h. The cells were then incubated overnight with antibodies against Col-II (1:200, 28459-1-AP, Proteintech, China), Sox9 (1:200, 67439-1-Ig, Proteintech, China), and aggrecan (ACAN) antibody (1:200, 13880-1-AP, Proteintech, China) at 4 °C.

Subsequently, the BMSCs were incubated at room temperature in the dark for 30 min with FITC-labelled goat anti-rabbit IgG (H + L) (1:200, A0562, Beyotime, China) and Actin-Tracker-Red-Rhodamine (1:200, C2207S, Beyotime, China). Nuclei were stained with DAPI for 5 min. The cells were observed with a Nikon inverted fluorescence microscope. (Nikon, Japan).

2.10. Establishment of a cartilage defect model

The experimental procedures involving animals in this investigation received approval (LAEC-2022-093) from the Institutional Animal Care and Use Committee (IACUC) of Zhujiang Hospital of Southern Medical University. New Zealand rabbits were randomly divided into 5 groups with 4 knee joints in each group at each time point. Briefly, after auricular marginal intravenous anaesthesia, the knee joints were exposed through a medial parapatellar approach, and a 4 mm × 2 mm cartilage defect was formed in the center of the non-weight-bearing area of the knee joint with a drill. Different SF-GMA/LKP solutions were injected into the defect, and UV irradiation was applied for 10 s to form glue *in situ*. The patella was then carefully repositioned to avoid hydrogel dislodgement. Finally, the wound was swabbed with iodophor and sutured closed. No material was implanted in the control group. Rabbits were sacrificed after 1 month and 3 months, and knee samples were obtained and subjected to micro-CT for detection, followed by pathology and immunohistochemical staining. Notably, Col-II and ACAN were subjected to immunohistochemical staining to evaluate the repair of cartilage defects. At the same time, Col-II immunofluorescence staining was performed on the relevant tissue samples to further determine the repair effect of cartilage defects.

2.11. Radiographic and histological evaluation of cartilage defect models

After 4 % paraformaldehyde was used to fix the cartilage defect in the knee joint, a micro-CT scan (ZKKS, China) and a three-dimensional reconstruction were performed. The trabecular bone count (Tb. N), bone surface area tissue-to-volume ratio (BS/TV), bone mineral density (BMD), bone surface area (BS), bone surface area-to-bone volume ratio (BS/BV), and bone volume fraction (BV/TV) were studied.

The cartilage defect knee joint samples were decalcified with EDTA decalcification solution (Lagena, China) for 1 month, dehydrated and cleared with gradient ethanol and xylene, and finally embedded in paraffin. The central part of the cartilage defect was excised for haematoxylin-eosin staining, safranin O-fast green staining, toluidine blue staining, immunohistochemical staining, and immunofluorescence staining.

3. Results

3.1. Preparation and characterization of peptide nanofiber hydrogels

A functional, self-assembled peptide nanofiber hydrogel was developed by covalently combining EKP with LIANAK (Scheme 1A). The chemical structure of the self-assembled peptides is shown in Fig. 1A. LKP was dissolved in ultrapure water, and the hydrogel was formed by simply adjusting the pH to neutral (Fig. 1B); this is because the hydrophobic amino acids (F) and hydrophilic amino acids (E and K) are

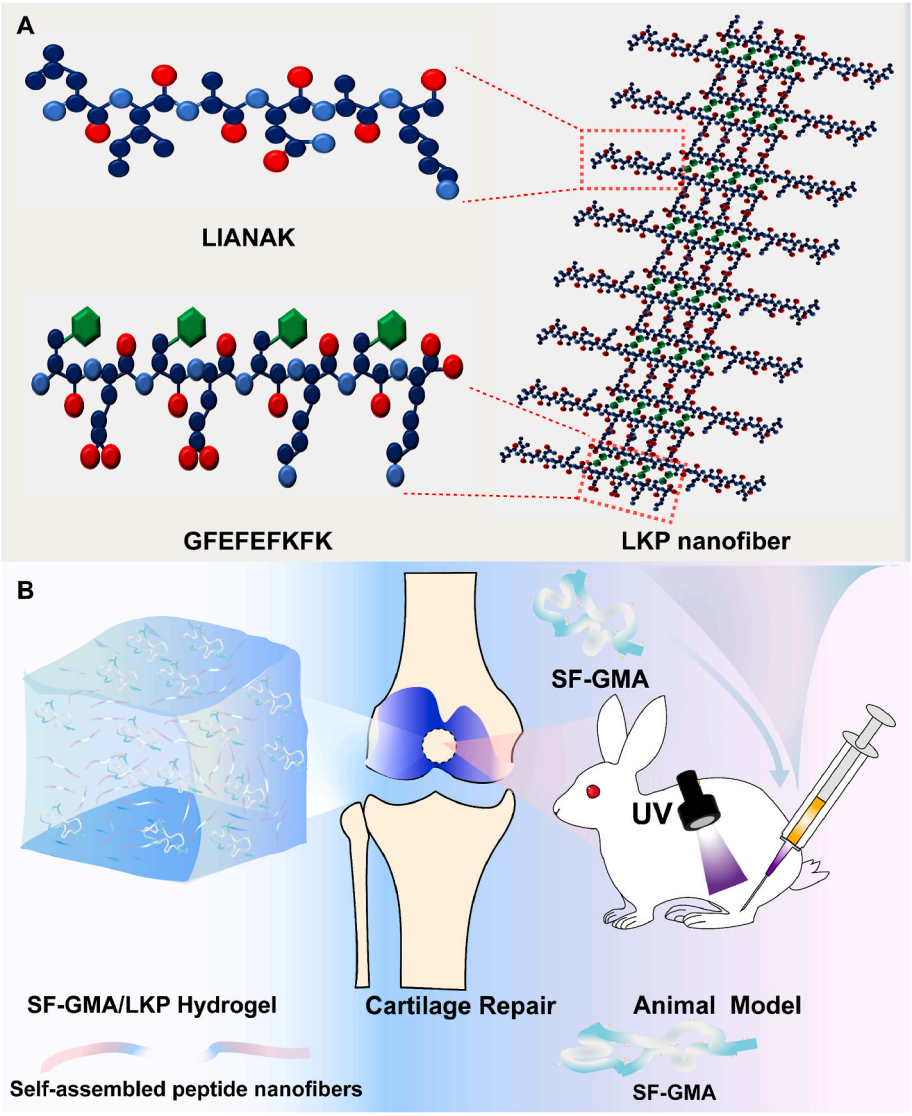

Scheme 1. Schematic diagram of the formation of self-assembled peptide nanofiber hydrogel **(A)**. Preparation of SF-GMA-LKP composite hydrogel scaffolds and a schematic diagram of cartilage repair **(B)**.

arranged alternately. The hydrophobic F quickly clumps together in the aqueous solution to lower the energy of the system, while the hydrophilic E and K residues are arranged in the outer layer of the self-assembly through electrostatic interactions [24,25]. A change in the solution pH intensifies the change in the reaction system and leads to the formation of the self-assembly hydrogels.

To demonstrate peptide assembly while preventing the drying process from potentially driving peptide assembly, we performed an AFM assay (Fig. 1C). We observed randomly distributed striped peptide nanofiber structures in both the EKP and LKP groups, confirming that the introduction of the LIANAK functional sequences does not affect the formation of self-assembled peptides.

The secondary structure of the peptide nanofiber hydrogel was studied by FTIR (Fig. 1D) and CD (Fig. 1E) analyses. Both LKP and EKP exhibited a typical β-sheet conformation in the CD spectrum, with a strong positive band at 195 nm and a strong negative band at 215 nm. FTIR spectra revealed the characteristic absorption peaks of the peptide nanofiber hydrogel. The characteristic absorption peaks of EKP and LKP are between 1623 and 1625 cm^{-1} and 1517 cm^{-1}, indicating that they have β-sheet structures. Moreover, the absorption peaks of EKP and LKP are between 1692 and 1694 cm^{-1}, suggesting that the assembled nanofibers can be formed by a parallel β-sheet.

To evaluate the microscopic characteristics of the peptide hydrogels, we performed TEM (Fig. 1 F) and SEM (Fig. 1 G) analysis. The results showed that the two peptide hydrogels formed uniform nanofiber structures of approximately 20–30 nm and interweaved with each other to form a loose porous network structure. This intricate network structure could stimulate cell adhesion and proliferation, as well as tissue regeneration [26].

3.2. *In vitro biocompatibility of the peptide nanofiber hydrogels*

BMSCs were coincubated with DMEM/F12 medium and peptide nanofiber hydrogels for 1, 4, or 7 days, and the biocompatibility of the hydrogels was detected via live-dead staining and CCK-8 assays. The results of live-dead staining are shown in Fig. 2A–C. Calcein-AM (AM) stains live cells with green fluorescence, and propidium iodide (PI) stains dead cells with red fluorescence. A difference in staining between live and dead cells was clearly observed after double-staining the superposition (Merge) of AM and PI. We can observe a large amount of green fluorescence representing living cells and only a very small amount of red fluorescence representing dead cells in the figure. The results showed that the LKP peptide nanofiber hydrogel had good biocompatibility.

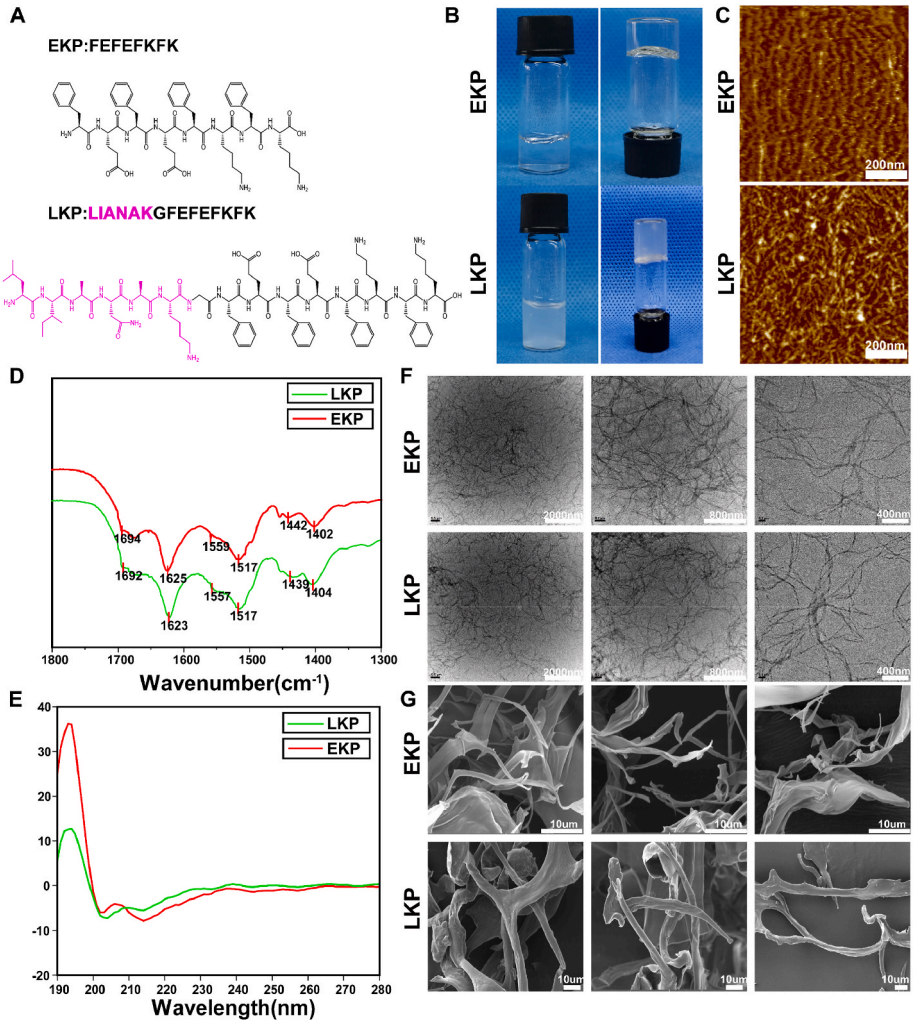

Fig. 1. Material characterization of peptide nanofiber hydrogels. Chemical structural formula of peptide nanofiber hydrogels **(A)**. Appearance of peptide nanofiber hydrogels **(B)**. AFM results of peptide nanofiber hydrogel **(C)**. FITR **(D)** and CD **(E)** results of peptide nanofiber hydrogels. TEM **(F)** and SEM **(G)** results of peptide nanofiber hydrogels.

Moreover, there was no significant difference in cell viability among the three groups on Day 1. On Days 4 and 7, however, the LKP group had substantially greater cell viability than the EFK and control groups (Fig. 2D). These results demonstrated that the peptide nanofiber hydrogel has good biocompatibility and can also promote cell growth and proliferation. LKP peptide nanofiber hydrogels form a loose three-dimensional network structure that mimics the extracellular matrix and provides a microenvironment for cell proliferation and growth. Moreover, LKP peptide nanofiber hydrogels can regulate cell proliferation by presenting LIANAK functional sequences, which play a role similar to that of TGF-β1.

3.3. Protein expression and immunofluorescence staining of peptide nanofiber hydrogels

The chondrogenic ability of the peptide nanofibers was evaluated by detecting the expression of Col-II, Sox9, and ACAN in BMSCs. Col-II and ACAN are typical cartilage markers, and Sox9 is an important transcription factor that can promote the expression of Col-II and ACAN and maintain the phenotype of articular chondrocytes [27–30]. BMSCs were cocultured with LKP or EKP peptide nanofiber hydrogels to investigate whether the introduction of functional sequences can promote cartilage. WB (Fig. 2E) and quantitative analysis (Fig. 2F and G) revealed that, compared with those in the blank group and the EFK group, the Col-II and Sox9 levels in the LKP group were significantly greater, which preliminarily confirmed the potential of the LKP peptide nanofiber hydrogel to promote chondrogenic differentiation of BMCSs. Surprisingly, Sox9 protein (Figs. S1A and B) and Col-II gene expression (Fig. S1C) in the LKP group reached the level of the TGF-β1 group, indicating that the introduction of the LIANAK functional sequence can mimic the biological function of TGF-β1. Moreover, we further evaluated the chondrogenic capacity of the LKP polypeptide nanofiber hydrogels by immunofluorescence staining (Fig. 3A–C, and E) and quantitative fluorescence analysis (Fig. 3B–D, and F). The expression levels of ACAN, Col-II, and Sox9 were highest in the LKP group, followed by those in the EKP group. We found that the addition of the EKP hydrogel alone can also promote an increase in cartilage regeneration-related proteins, presumably related to its porous nanofiber structure, which is beneficial for the proliferation of BMSCs. Moreover, the introduction of the LKP functional sequence significantly promoted the expression of chondrogenic markers in BMSCs, indicating that covalent binding of LKP and EKP did not affect their biological activity.

In contrast to TGF-1, which has a tertiary structure suitable for exerting biological activity, LIANAK mimetic peptides are smaller and have uncomplicated structure modifications, allowing them to retain excellent biological activity during covalent binding. Due to its interwoven nanonetwork structure, the LKP hydrogel aids in simulating the

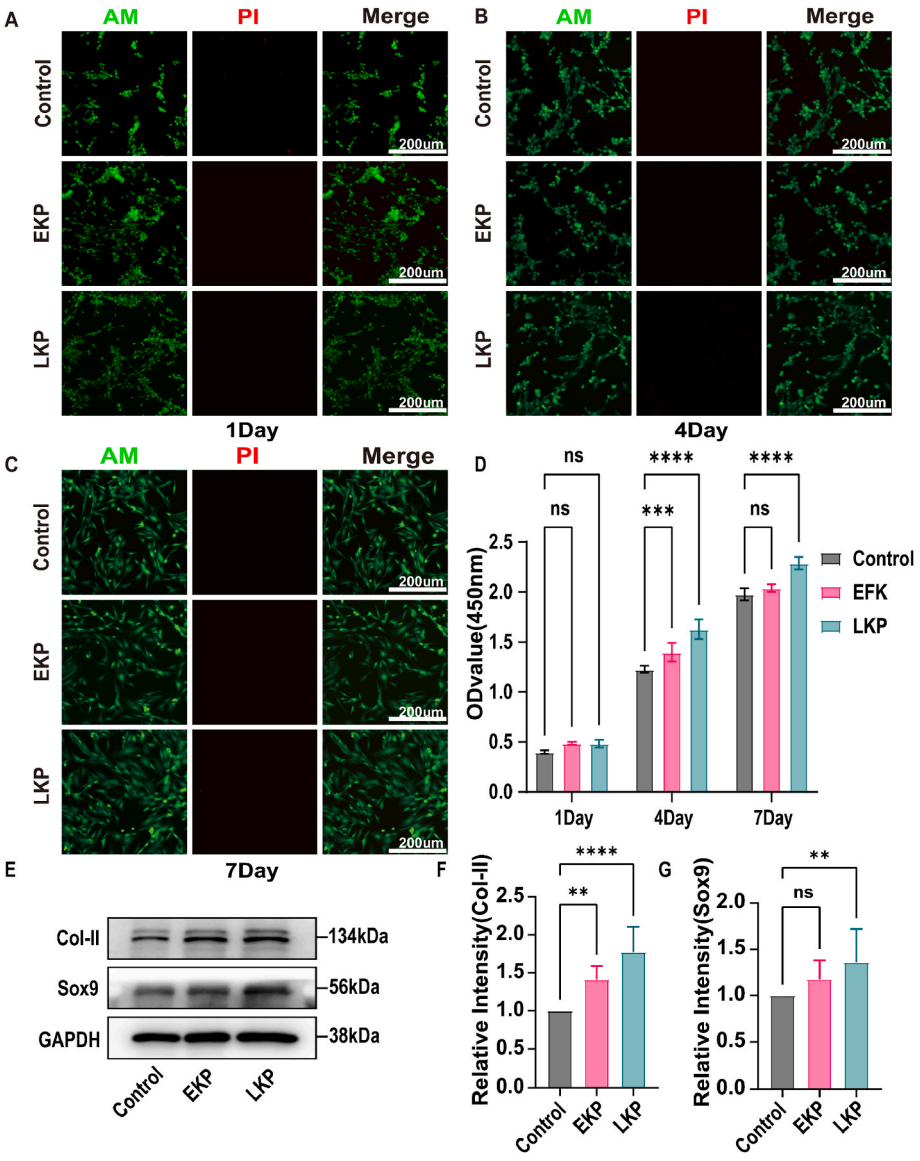

Fig. 2. Effect of peptide nanofiber hydrogels on BMSCs. Live-dead staining **(A–C)** and CCK-8 **(D)** results of BMSCs exposed to different peptide nanofiber hydrogels on days 1, 4, and 7. WB **(E)** results and quantitative analysis of Col-II **(F)** and Sox9 **(G)** of BMSCs treated with different peptide nanofiber hydrogels. Results were expressed as means ± SD; ns means no significant difference. *P < 0.05, * *P < 0.01, * * *P < 0.001,* * * *P < 0.0001.

microenvironment of BMSC reactions and, simultaneously, exerts the biological function of TGF-β1 mimetic peptide, thereby promoting BMSCs cartilage differentiation.

4. Preparation and characterization of the SF-GMA and SF-GMA/LKP hydrogel scaffolds

By mixing SF-GMA and LKP peptide nanofiber hydrogels in a certain proportion, injectable SF-GMA/LKP composite hydrogel scaffolds were developed for cartilage regeneration (Fig. S2A and Video 1). Due to its biocompatibility, SF has been extensively utilized in cosmetics, trauma, and other sectors. However, the use of SF is limited because it is insoluble or slightly soluble in water. We prepared SF-GMA by reacting GMA with SF. SF-GMA has good solubility and a light curing effect. Successful SF-GMA was evaluated by 1H NMR (Fig. 4A) and FTIR (Fig. 4B) analysis. The absorption peaks of amides I, II, and III appeared at 1639, 1512, and 1234 cm^{-1} for both SF and SF-GMA, respectively. At 1239 cm^{-1}, a faint spectral band corresponding to SF-GMA can be observed, which is caused by the ring opening of the epoxy group of GMA. To further confirm that GMA was successfully introduced into SF, we further evaluated it by 1H NMR. The results show that the characteristic resonances of vinyl methacrylate appear at $\delta = 6.26$ and 5.6–5.8 ppm, and the characteristic methyl resonance of GMA is also found at $\delta = 1.8$ ppm. The above results showed that we have successfully introduced GMA groups to modify SF.

Supplementary video related to this article can be found at https://doi.org/10.1016/j.mtbio.2024.100962

For all four SF-GMA/LKP solutions at the same temperature and frequency from 0.1 to 10 rad/s, the loss modulus G″ is greater than the storage modulus G' (Fig. 4D–G). This means that the solutions are viscoelastic. At a frequency of 100 rad/s, G″ is greater than G′ for the SF-GMA/LKP0 group, indicating that the SF-GMA/LKP0 group is still in the liquid state, while G′ is greater than G″ for the SF-GMA/LKP10 and SF-GMA/LKP20 groups, indicating that the two groups are transformed from viscoelastic liquids to solids. This confirmed, to some extent, that the doping of LKP affected the conformational transition of SF-GMA and improved the strength of the composite scaffolds.

Moreover, the G′ and G″ of the four groups of SF-GMA/LKP solutions were lower at 37 °C than at 25 °C, which could be attributed to the fact that the interactions between solute molecules weakened as the

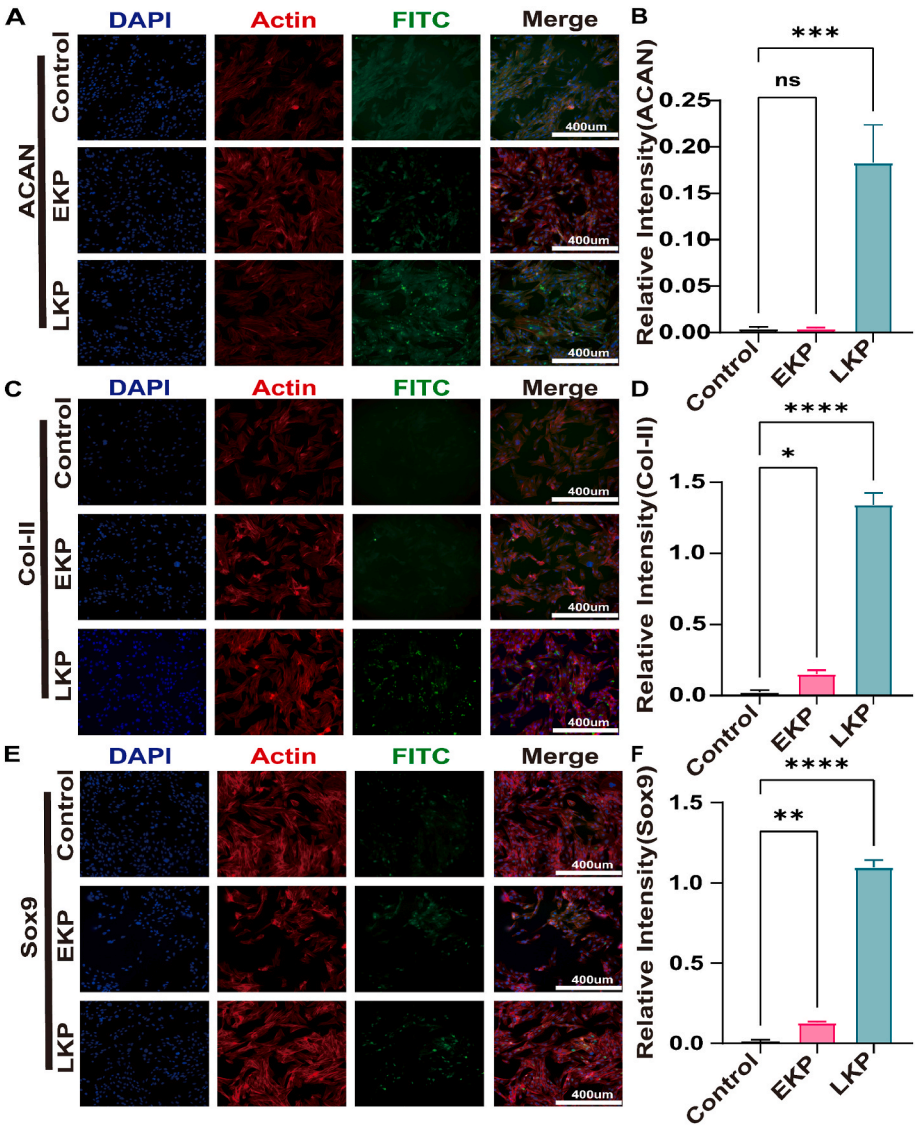

Fig. 3. Effect of peptide nanofiber hydrogels on BMSCs. Representative images of immunofluorescence of ACAN **(A)**, Col-II **(C)**, and Sox9 **(E)** of BMSCs treated with different peptide nanofiber hydrogels. Immunofluorescence intensity analysis of ACAN **(B)**, Col-II **(D)**, and Sox9 **(F)** of BMSCs treated with different peptide nanofiber hydrogels. Results were expressed as means ± SD; ns means no significant difference. *P < 0.05, * *P < 0.01, * * *P < 0.001,* * * *P < 0.0001.

temperature increased, decreasing the structure of the gels. Notably, at a frequency of 100 rad/s, the G′ of the SF-GMA/LKP10 and SF-GMA/LKP20 groups was close to 10^4 Pa, but there was almost no difference between the two, suggesting that excessive doping of LKP does not synchronously improve the mechanical properties of composite scaffolds.

During the 28-day *in vitro* degradation experiment, no sudden or rapid deterioration was observed; instead, the degradation rate of each of the four groups of materials increased gradually (Fig. 4C). Nearly 50 % of the materials in the four groups were still not degraded after 28 days of degradation, but with the increase in the proportion of peptide nanofiber hydrogel, the degradation rate of the composite scaffold accelerated, which was due to the addition of the peptide nanofiber hydrogel improving the microstructure of SF-GMA.

FTIR results revealed that the SF-GMA/LKP0 had an absorption peak at 1643 cm^{-1}, indicating that there was random curl in the internal structure of the SF-GMA/LKP0, while the SF-GMA/LKP5 had an absorption peak at 1636cm-1, which was a typical β-sheet structure, suggesting that the SF-GMA/LKP5 had an obvious change in the internal structure of SF-GMA (Fig. 5A). It is worth mentioning that the SF-GMA/LKP10 and SF-GMA/LKP20 exhibit typical α-helix structures (1651 cm^{-1} and 1655 cm^{-1}), suggesting that excessive doping of LKP does not further affect the internal structure of SF-GMA.

We evaluated the 24-h swelling performance of the four SF-GMA/LKP scaffolds (Fig. 5B). The composite hydrogel scaffolds in the 4 groups swelled slowly in the first 5 h and increased rapidly in 5–16 h. The swelling rates of the SF-GMA/LKP0, SF-GMA/LKP5, SF-GMA/LKP10, and SF-GMA/LKP20 at 24 h were 421 %, 519 %, 503 %, and 487 %. The results revealed that doping LKP can improve the water absorption capacity of composite hydrogel scaffolds, but excessive doping cannot simultaneously enhance the swelling capacity of scaffolds.

The microstructure of the four SF-GMA/LKP hydrogel scaffolds is shown in Fig. 5C. The addition of LKP significantly affects the pore size of the SF-GMA internal structure. The pore size of SF-GMA/LKP5 is the smallest, while the pore size of SF-GMA/LKP10 and SF-GMA/LKP20 begins to increase gradually, which also indicates that the excessive addition of LKP does not simultaneously improve the microstructure of the scaffolds. The increase in pore size leads to an increase of water absorption capacity, swelling performance, and degradation rate.

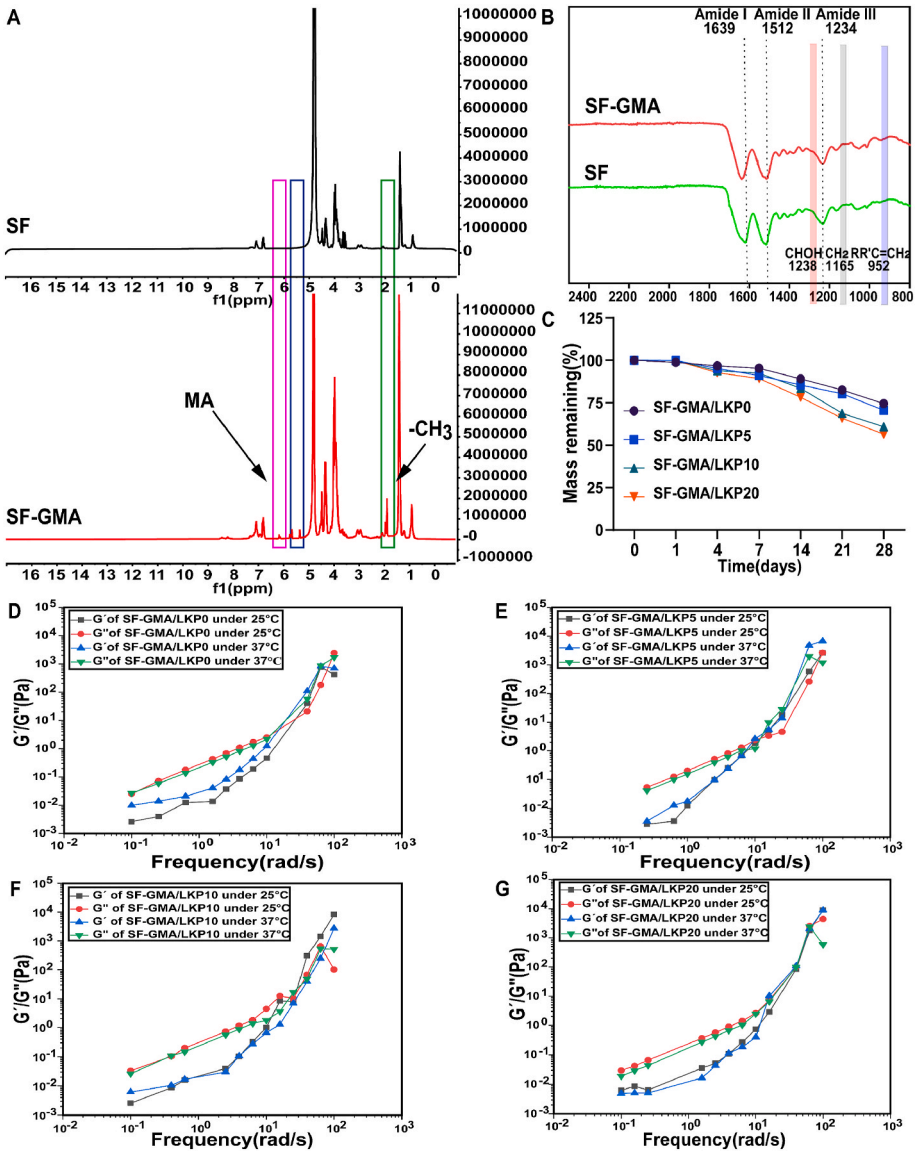

Fig. 4. Characterization of SF-GMA and SF-GMA/LKP scaffolds. **(A)** Nuclear Magnetic Resonance Hydrogen Spectra of SF-GMA. **(B)** FTIR of SF-GMA. **(C)** Degradation curves of different SF-GMA/LKP scaffolds. **(D–G)** Rheological properties of different SF-GMA/LKP solutions.

4.1. Cytocompatibility of the SF-GMA/LKP composite hydrogel scaffolds in vitro

BMSCs were cocultured with four different ratios of SF-GMA/LKP composite hydrogels for 1, 4, or 7 days. CCK-8 staining (Fig. 6A) and live-dead staining (Fig. 6B–D) were both used to assess the biocompatibility of the composite hydrogels. After 1 day of coculture, the data indicated that there was no discernible difference in CCK-8 expression between the groups. However, after 4 and 7 days of cocultivation, the capacity of the composite scaffolds to promote BMSC proliferation increased as the LKP hydrogel concentration increased. The cells in each group were healthy during the same period, and very few dead cells were observed. The outcomes demonstrated the high biocompatibility of the composite hydrogel scaffolds and their ability to support BMSC development and expansion.

4.2. Adhesion and three-dimensional culture of the SF-GMA/LKP composite hydrogel scaffolds in vitro

We cocultured the composite scaffolds with BMSCs for one day to assess adhesion. After that, the tissues were fixed with 4 % paraformaldehyde, subjected to gradient dehydration, carbon dioxide critical point drying, and SEM observation (Fig. 6E). The outcomes demonstrated that BMSCs were able to adhere to and proliferate on the composite hydrogel scaffolds. In addition, BMSCs were mixed with the SF-GMA/LKP solutions and photocured to form hydrogel, and then cultured in 3-D (Fig. 7). The results also revealed that BMSCs could survive in four groups of SF-GMA/LKP hydrogel scaffolds, which further confirmed their excellent biological safety. Moreover, with increasing peptide nanofiber hydrogel concentrations, the structure of the composite scaffold underwent microscopic changes, which is favourable for cell growth. We believe that the addition of peptide nanofiber hydrogels significantly changes the microstructure of SF-GMA. We hypothesized that this difference may be due to the addition of peptides through hydrophobic and hydrogen bonding interactions leading to a simple SF-GMA conformation transition, resulting in a more porous and structurally stable micromorphology, which is consistent with the findings of previous studies [23].

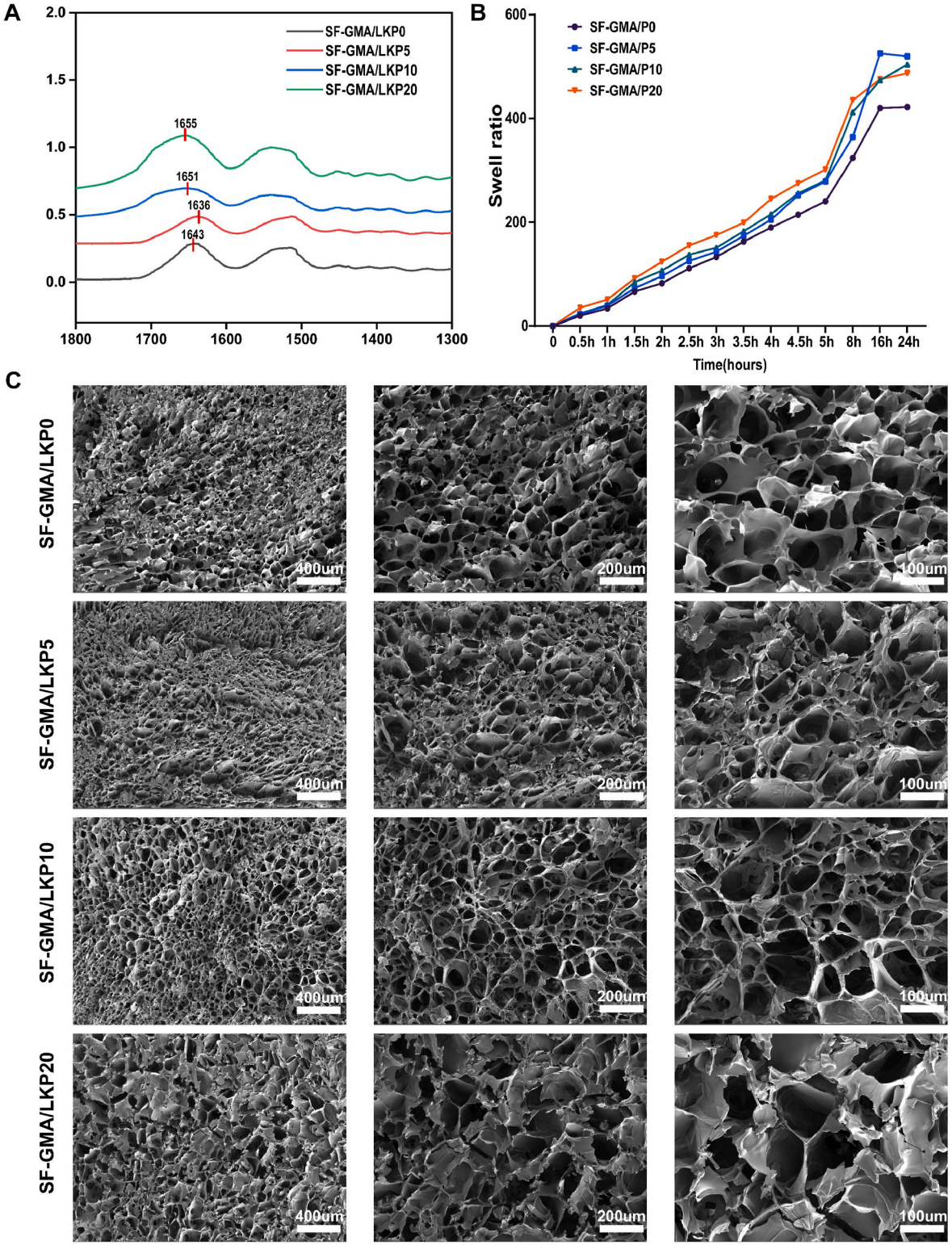

Fig. 5. Characterization of SF-GMA and SF-GMA/LKP scaffolds. **(A)** FTIR results of SF-GMA/LKP. **(B)** Swelling results of four SF-GMA/LKP hydrogel scaffolds. **(C)** SEM results of four SF-GMA/LKP hydrogel scaffolds.

4.3. Protein expression and immunofluorescence staining of the SF-GMA/LKP composite hydrogel scaffolds

WB (Fig. 8A) and quantitative analysis (Fig. 8B and C) demonstrated that the SF-GMA/LKP20 and SF-GMA/LKP10 groups exhibited the highest levels of Col-II and Sox9 expression relative to those in the control group. These findings suggested that appropriate doping of polypeptide nanofiber hydrogels may play a role in promoting cartilage differentiation. Moreover, immunofluorescence (Fig. 8D–F) and quantitative analysis (Fig. 8G–I) revealed that the SF-GMA/LKP20 and SF-GMA/LKP10 groups contained the highest levels of ACAN, Sox9, and Col-II expression. There was no significant difference in the expression

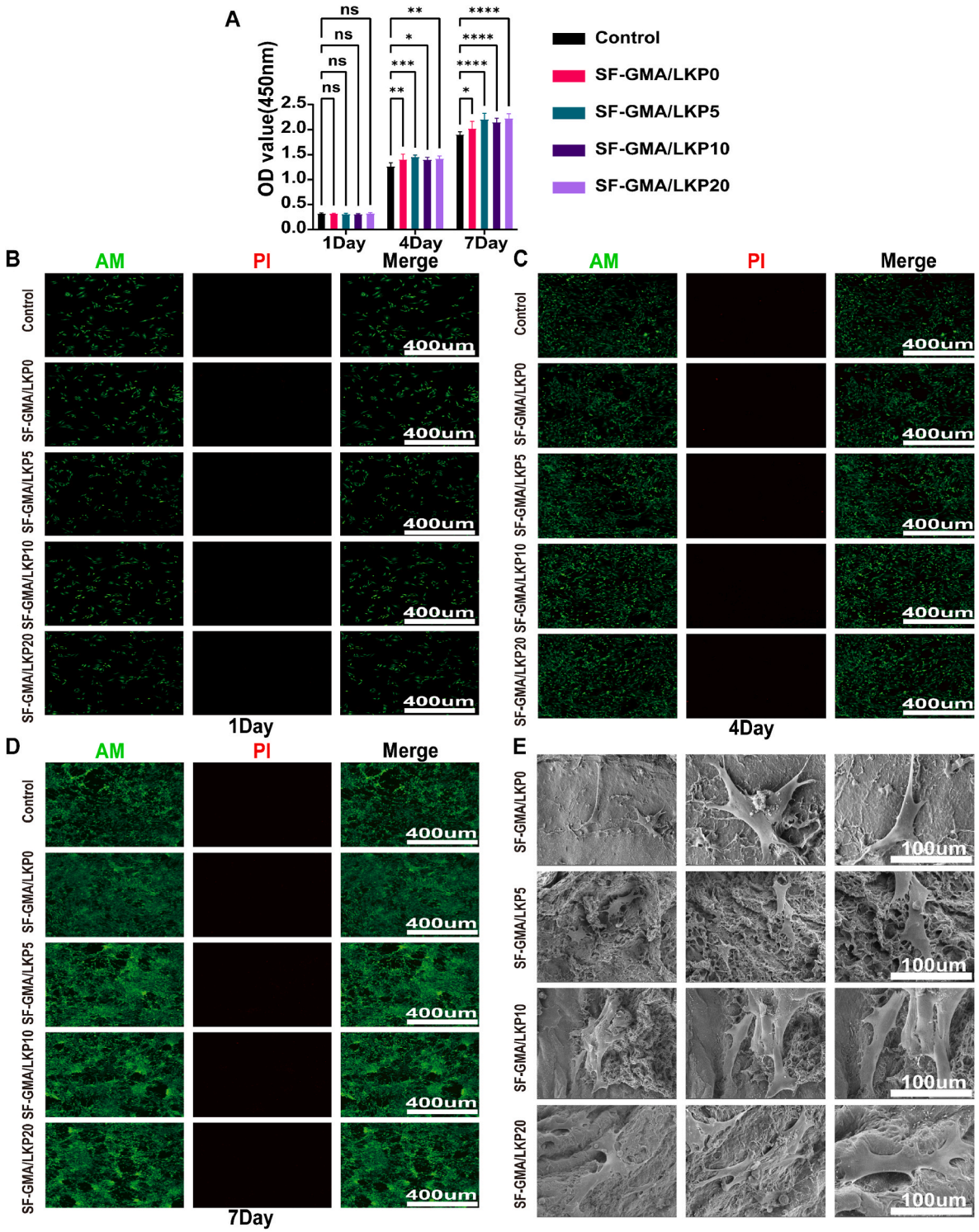

Fig. 6. Biocompatibility of different SF-GMA/LKP hydrogel scaffolds. (A) CCK-8 results of BMSCs exposed to different SF-GMA/LKP hydrogel scaffolds for 1, 4, and 7 days. (B–D) Live-dead results of BMSCs exposed to different SF-GMA/LKP hydrogel scaffolds for 1, 4, and 7 days. (E) SEM results of BMSCs seeded on different SF-GMA/LKP scaffolds. Results were expressed as means ± SD; ns means no significant difference, *P < 0.05, * *P < 0.01, * * *P < 0.001,* * * *P < 0.0001.

levels of the pertinent proteins between the control group and the SF-GMA/LKP0 group not treated with the peptide hydrogels. These results further confirmed that the incorporation of the LKP hydrogel promoted chondrogenic and osteogenic differentiation effects.

4.4. Biocompatibility, histology and immunohistochemistry analysis of the SF-GMA/LKP composite hydrogel scaffolds in vivo

The ability of the SF-GMA/LKP composite hydrogel scaffold to repair cartilage defects was investigated by modelling cartilage defects in rabbit knee cartilage. In the present study, four SF-GMA/LKP composite hydrogels were injected *in situ* and cured *in situ* with UV light (Fig. S2B

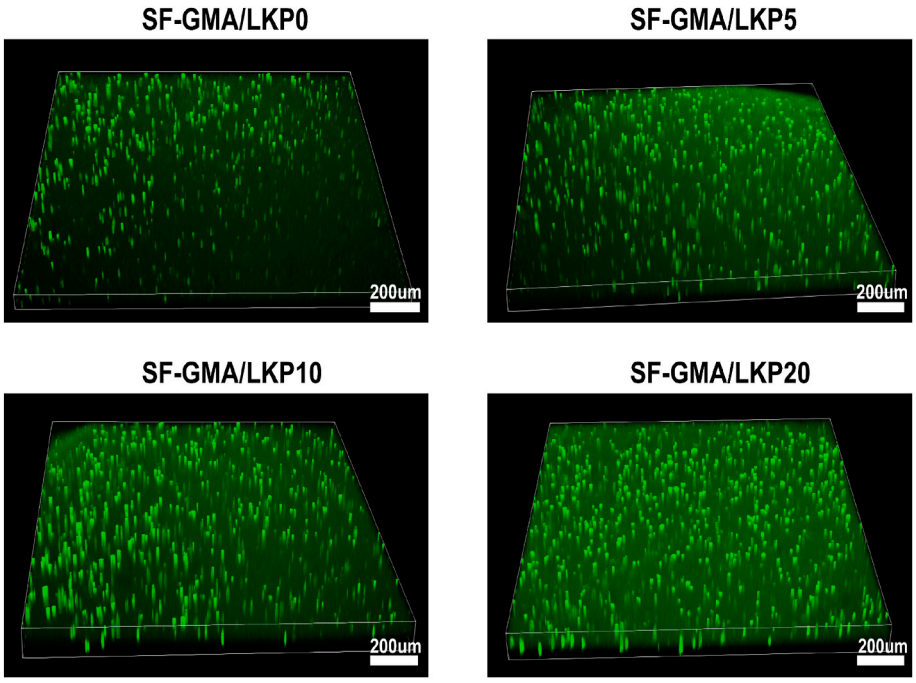

Fig. 7. 3D culture results of BMSCs on different SF-GMA/LKP hydrogel scaffolds.

and Video 2). Knee joint specimens and visceral organ specimens were obtained at 1 and 3 months, respectively, to evaluate the biocompatibility and repair effects of the various cartilage defects.

Supplementary video related to this article can be found at https://doi.org/10.1016/j.mtbio.2024.100962

HE staining was performed on the obtained heart, liver, spleen, lung, and kidney samples (Fig. S3). We did not find obvious inflammatory infiltration, such as neutrophils, or the formation of multinucleated giant cells. All organs maintained normal structures. These findings were consistent with the *in vitro* results, indicating that the SF-GMA/LKP composite hydrogel scaffold had good biocompatibility.

We evaluated the effect of the four materials on subchondral bone using micro-CT (Fig. 9A) and found that the repair of subchondral bone repair was dependent on endochondral osteogenesis. The

control and SF-GMA/LKP0 groups showed only a small amount of mineralization of bone deposits at 1 month, and at 3 months, the amount of bone at the defect site was increased compared to that at the previous site, but the bone-cartilage interface was very concave. Subchondral bone augmentation was greater in the SF-GMA/LKP5 group than in the control and SF-GMA/LKP0 groups, with increased osteogenesis within the cartilage of the central round defect. The SF-GMA/LKP10 and SF-GMA/LKP20 composite scaffold groups already exhibited optimal subchondral bone repair at 1 month, and at 3 months the subchondral bone had been largely repaired, the bone-cartilage interface was flat, and the central round defect had been completely filled. Quantitative analysis (Fig. 9B–G) of the subchondral bone repair process showed that the BV/TV, BS/TV, BS, BS/BV, BMD, and Tb.N. of the SF-GMA/LKP10 and SF-GMA/LKP20 composite scaffold groups were superior to those of the other groups, which indicated that these two groups had the best results in terms of subchondral bone repair.

We evaluated the regeneration of cartilage defects in knee tissue samples by HE staining, gross observation, and cartilage-related characteristic staining (Fig. 10A and B). One month after cartilage defect surgery, the central portion of the cartilage defect in the control group was filled with only a small quantity of fibrous-like tissue, and the cartilage defect border was clearly visible, with no discernible signs of cartilage regeneration. Different degrees of cartilage defect repair were observed in the remaining four groups, and the SF-GMA/LKP10 and SF-GMA/LKP20 groups exhibited the best cartilage repair effect. The new cartilage was smooth and slightly protruded from the normal plane, and the border of the surrounding cartilage defect gradually closed. Surprisingly, the SF-GMA/LKP composite scaffolds were still observed in some images, indicating that they still played a role, which was consistent with our *in vitro* degradation results. Three months after cartilage defect surgery, the cartilage defects in the control group exhibited more fibrous tissue-like formations and no discernible new cartilage. Between the SF-GMA/LKP10 and SF-GMA/LKP20 composite scaffold groups, the defect boundary disappeared, the new cartilage was smooth, and the morphology of the new cartilage was consistent with that of the normal cartilage, indicating that the regenerated cartilage was mature hyaline cartilage. Moreover, there was no evidence of residual SF-GMA/LKP composite hydrogel scaffold, indicating that the scafford had been completely degraded.

Immunofluorescence (Fig. 11) and immunohistochemistry (Fig. 12) were subsequently used to determine the effect of the SF-GMA/LKP composite hydrogel scaffolds on the expression of related cartilage proteins in cartilage defects. We observed that the cartilage defects in the control group and in the SF-GMA/LKP0 composite hydrogel scaffold groups had not been repaired after 3 months because there was no LKP incorporation; most of the defects were nonspecifically stained fibrous tissue, and no obvious chondrocytes were found. However, because of the greater concentration of LKP in the SF-GMA/LKP10 and SF-GMA/LKP20 composite scaffold groups, there were specific stained hyaline chondrocytes, and the border of the cartilage defect was almost indistinguishable from the normal border.

5. Discussion

Regeneration of cartilage defects is still a tricky clinical challenge [31]. The repair of cartilage damage depends on the appropriate concentration of TGF-β1 [32]. Unfortunately, there is insufficient blood supply in the joint cavity to provide sufficient concentrations of TGF-β1 for cartilage repair. Exogenously loaded TGF-β1 is prone to rapid release, leading to inadequate cartilage repair [33]. Moreover, TGF-β1 requires a certain spatial structure to exert its biological function, and it is easily enzymatically denatured during delivery with other materials,

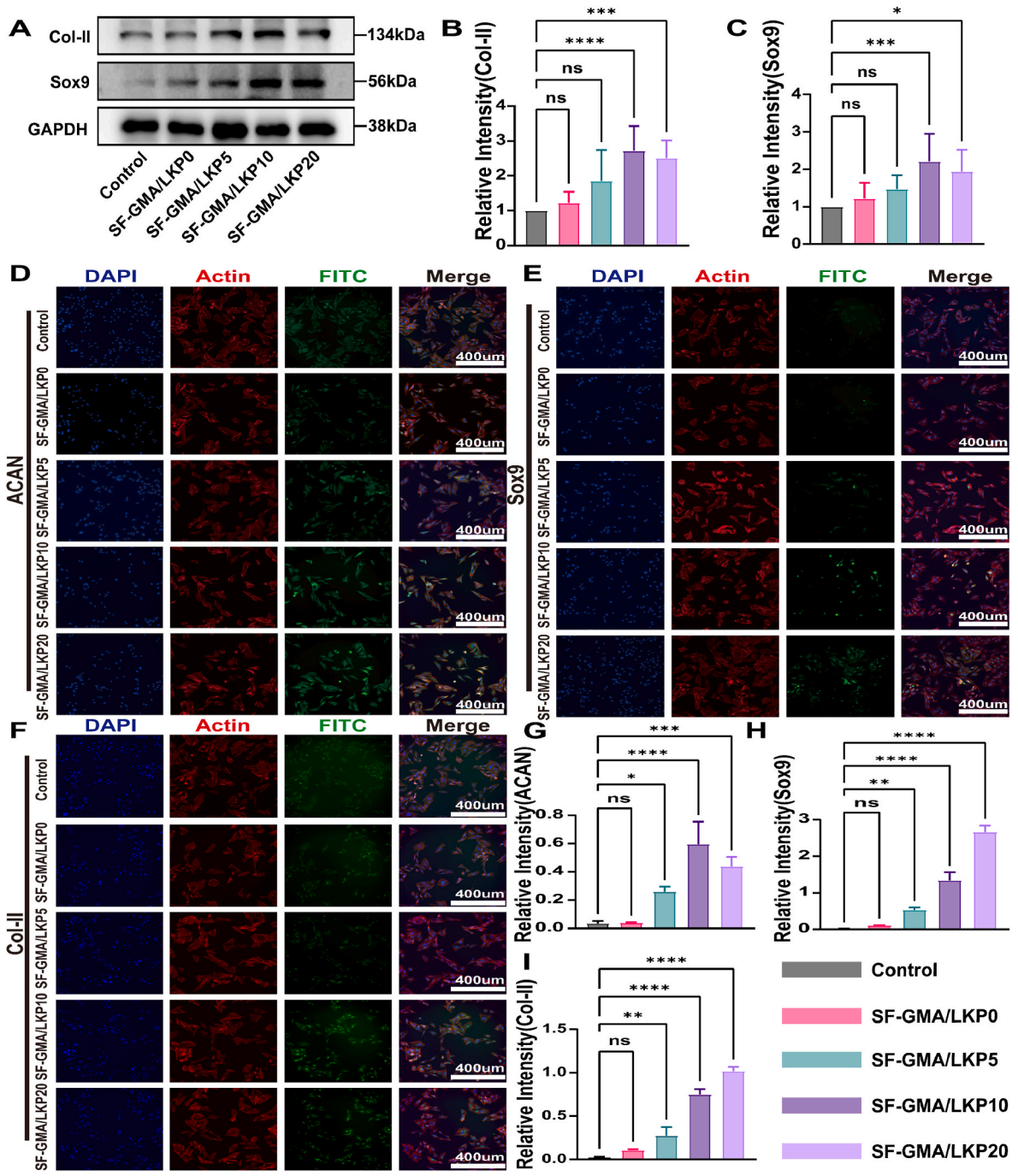

Fig. 8. Effects of different SF-GMA/LKP hydrogel scaffolds on bone marrow mesenchymal stem cells. Western blot results **(A)** and quantitative analysis of Col-II **(B)** and Sox9 **(C)** of BMSCs treated with different SF-GMA/LKP hydrogel scaffolds. **(D–F)** Immunofluorescence-representative images of ACAN, Sox9, and Col-II of BMSCs treated with different SF-GMA/LKP hydrogel scaffolds. **(G–H)** Immunofluorescence intensity analysis of ACAN, Sox9, and Col-II of BMSCs treated with different SF-GMA/LKP hydrogel scaffolds. Results were expressed as means ± SD; ns means no significant difference, *P < 0.05, * *P < 0.01, * * *P < 0.001,* * * *P < 0.0001.

which limits its use to a certain extent. LIANAK is a mimetic peptide of TGF-β1 that has a simple spatial structure and simultaneously promotes cartilage regeneration, which makes it an ideal substitute for TGF-β1. However, the application of LIANAK alone has the same problem of rapid diffusion. Therefore, there is a need to develop a system for the slow-release delivery of LIANAK.

We first designed a self-assembling peptide hydrogel (LKP) as a vehicle for administering LIANAK. FEFEFKFK acts as a self-assembly motor, and LIANAK has a corresponding biological function. These two residues are linked by glycine to protect the spatial structure of LIANAK from self-assembly sequences. FTIR, CD, SEM, and TEM confirmed that LKP could form nanofibers in β-sheet mode after simple pH adjustment. Live-dead staining and CCK-8 results confirmed that the LKP peptide nanohydrogel has good biocompatibility. Moreover, from the CCK-8 results, we found that there was no difference among the three groups after they were cocultured for 1 day, whereas the LKP group exhibited the greatest increase in cell proliferation over time, which may be due to the gradual degradation and release of the LKP hydrogel. In addition, WB and immunofluorescence results confirmed the excellent prochondrogenic ability of the LKP peptide nanofiber hydrogels. Although some of the EKP hydrogels also promoted chondrogenic activity in several chondrogenic indexes (Col-II and Sox9), we

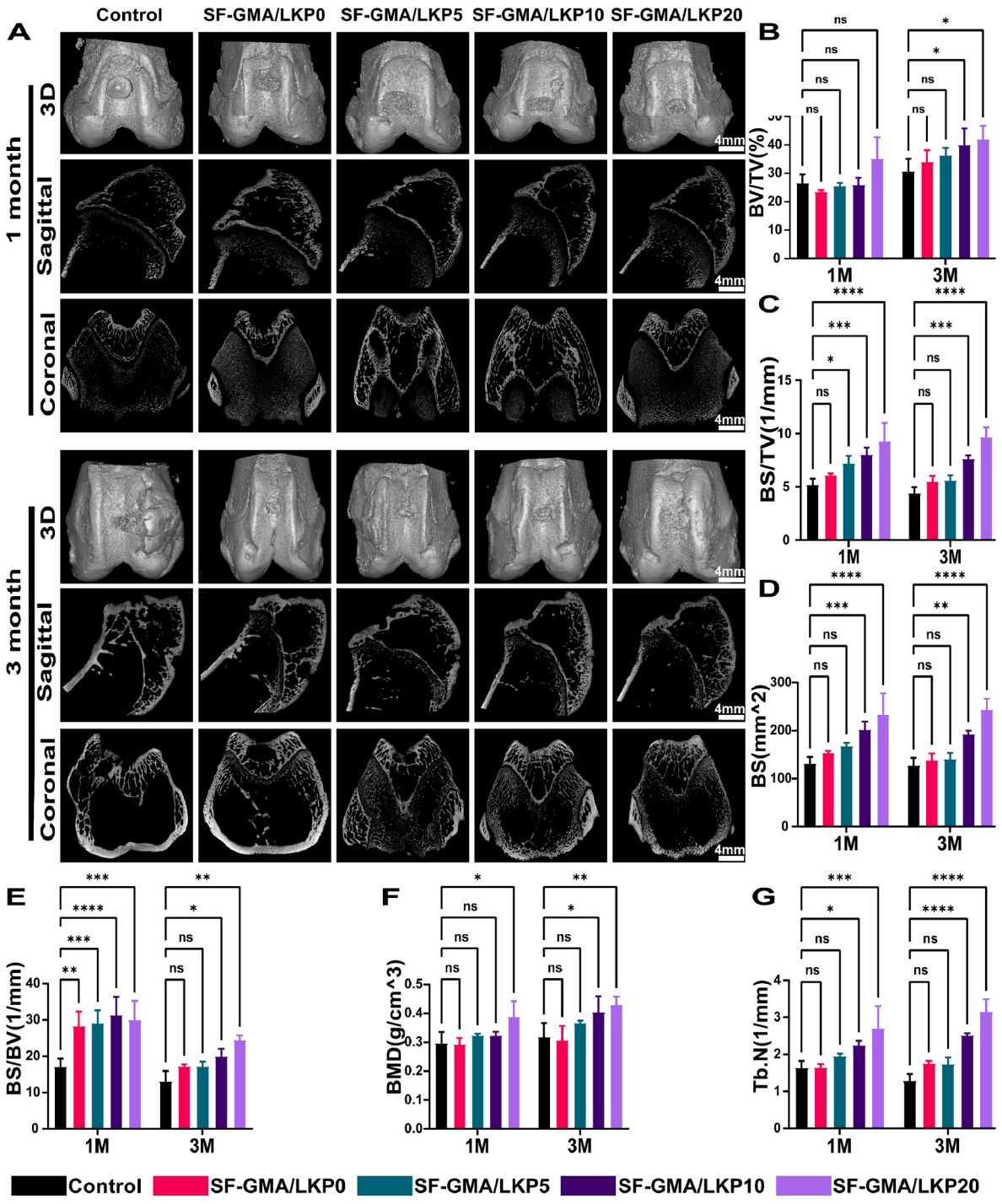

Fig. 9. Micro-CT results of different SF-GMA/LKP hydrogel scaffolds on cartilage defects. Micro-CT representative image of the cartilage defect model **(A)**. Quantitative analysis of subchondral bone based on micro-CT images **(B–G)**. Results were expressed as means ± SD; ns means no significant difference. *P < 0.05, * *P < 0.01, * * *P < 0.001,* * * *P < 0.0001.

hypothesized that this was because the EKP hydrogels also possessed a loose and porous fibrous structure, which was conducive to the proliferation of BMSCs. However, the chondrogenic ability of the LKP hydrogels was much greater than that of the EKP hydrogels, indicating that the covalent binding of LIANAK to FEFEFKFK did not affect its biological function.

Although the LKP hydrogel has good cartilaginous properties, we found that its mechanical properties are poor and tha it is easy to break in practice; therefore, it is impossible to carry out relevant mechanical property tests. Cartilage mainly plays a load-bearing and buffer role, while LKP hydrogels are not conducive to adhesion or mechanical properties in cartilage defects due to a lack of viscoelasticity, which limits their use. Based on the results of previous investigations, the conformation of SF can be transformed by hydrogen bonding and hydrophobic interactions when polypeptides or small molecules are incorporated into SF, and a stable hydrogel can be gradually formed within 5–30 min [22,23]. For practical application in cartilage defect repair, hydrogels that can be filled *in situ* immediately and solidified stably are needed. Therefore, we report a novel composite hydrogel scaffold formed by incorporating an LKP self-assembled polypeptide into

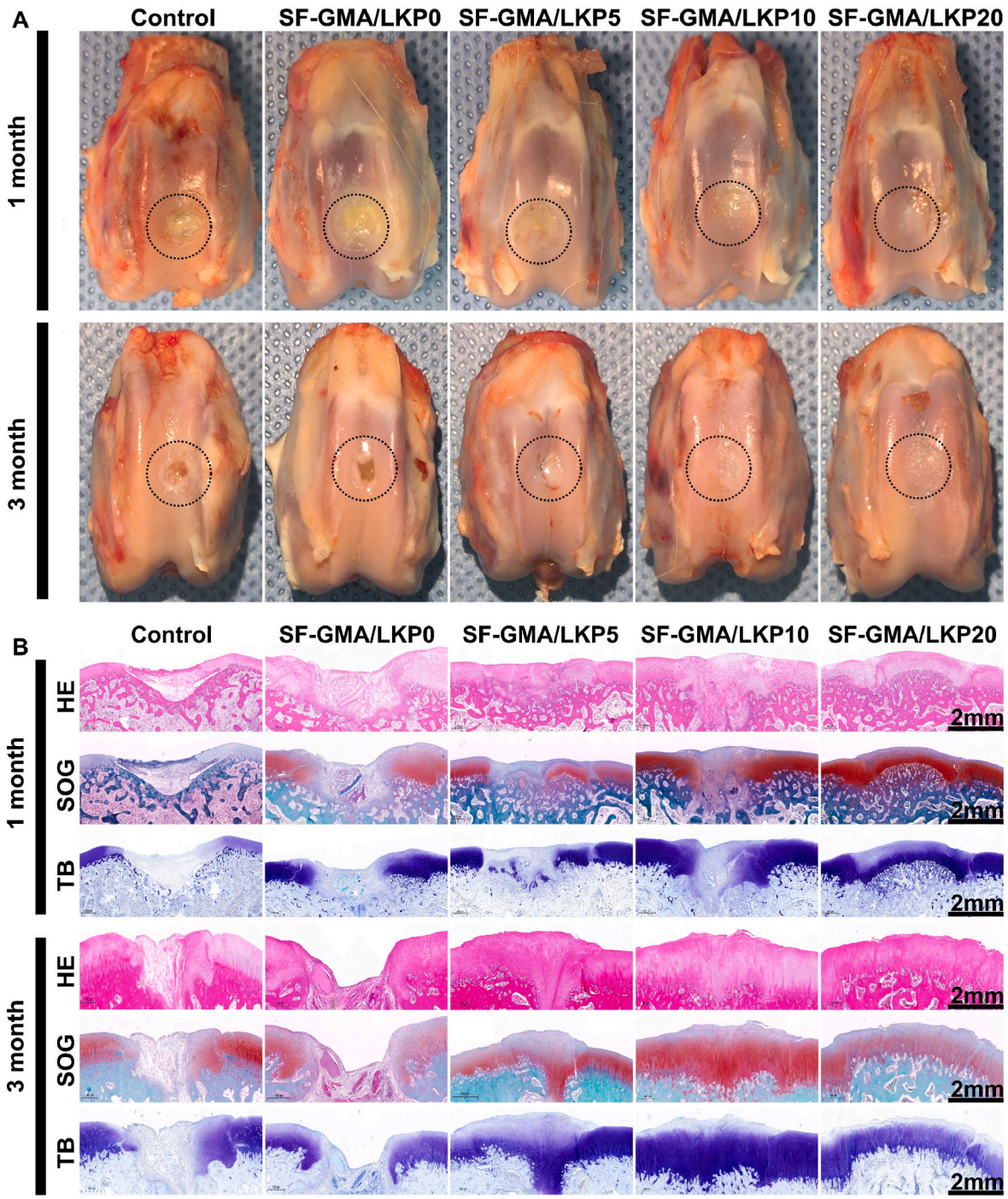

Fig. 10. *In vivo* results of different SF-GMA/LKP hydrogel scaffolds on rabbit cartilage defect models. Appearance of different SF-GMA/LKP hydrogel scaffolds acting on rabbit cartilage defect models at 1 m and 3 m **(A)**. HE staining, Safranin O-fast green staining, and toluidine blue staining of rabbit cartilage defect models with different SF-GMA/LKP hydrogel scaffolds **(B)**.

SF-GMA. The composite hydrogel stent can be immediately solidified under the action of ultraviolet light so that the residence time of the LKP is prolonged and the defect that the SF needs to wait for a long time is overcome. From the degradation time and rheological results, we find that it is not the case that the more LKP peptides are doped into SF-GMA, the stronger their interaction is. Therefore, we wanted to determine the optimal ratio of the two parameters to obtain the best cartilage restoration results. Since the LKP peptide doped into SF-GMA was not covalently bound, this did not affect its biocompatibility, and our results similarly confirmed the good biocompatibility of SF-GMA/LKP. WB and immunofluorescence further confirmed that SF-GMA incorporation did not affect the chondrogenic ability of the LKP.

Since subchondral bone is often absent in most cases of cartilage defects, subchondral bone repair also helps to support for cartilage defect repair [34–36]. Micro-CT results revealed that SF-GMA/LKP was helpful for subchondral bone repair, and SF-GMA/LKP10 and SF-GMA/LKP20 exhibited the greatest ability to promote subchondral bone repair. Gross observation and staining results revealed that the new cartilage in the SF-GMA/LKP10 and SF-GMA/LKP20 groups was smoother than that in the control group, and the cartilage defect boundary was almost blurred.

This study has several limitations. First, we did not explore the

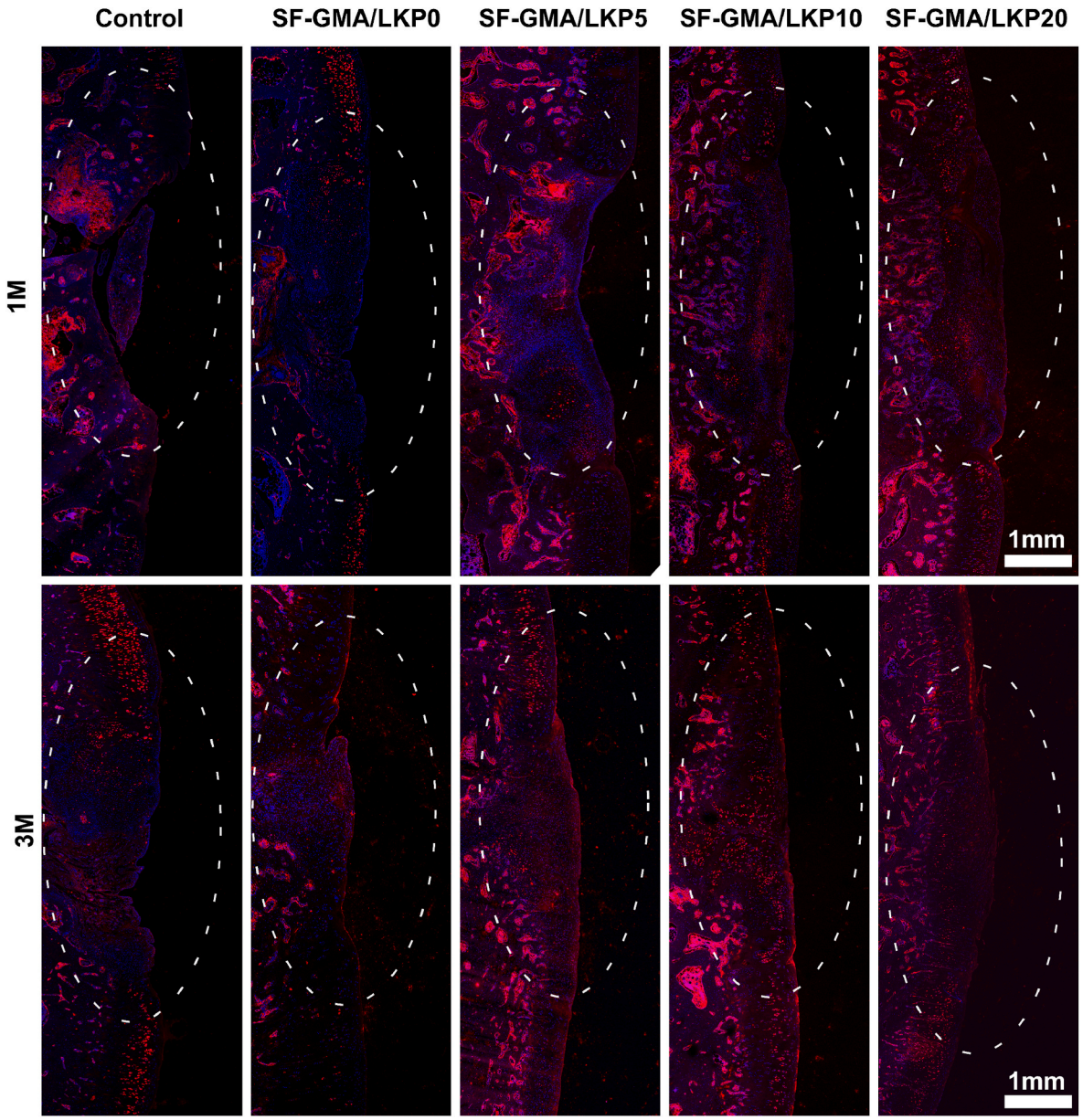

Fig. 11. Immunofluorescence staining of Col-II in rabbit cartilage defects of 1 m and 3 m treated with different SF-GMA/LKP hydrogel scaffolds.

mechanism associated with the LKP hydrogel mimicking TGF-β1. Additionally, we only demonstrated that LKP can fully mimic TGF-β1 function *in vitro*, and did not verify it *in vivo*, which may be insufficient. LKP hydrogel can mimic the function of TGF-β1, and excessive activation may lead to cartilage hypertrophy; moreover, we did not test relevant hypertrophy-related indexes. Therefore, we should further investigate this phenomenon in depth in future experiments.

6. Conclusion

Here, we report an LKP hydrogel that uses EFK as a self-assembly driving force to deliver the TGF-β1 mimetic peptide LIANAK. The LKP hydrogel has a typical nanofibrous structure and has been demonstrated to have good biocompatibility and excellent prochondrogenic ability in *in*experiments, suggesting that the introduction of EFK does not affect the biological activity of LIANAK. Based on the principle that peptides can induce SF conformational transition to gradually form a stable hydrogel within 30 min, we developed a composite scaffold, SF-GMA/LKP, that synergistically assembles SF-GMA rather than SF with LKP. The SF-GMA/LKP scaffold overcomes the problems associated with the poor mechanical properties of the LKP hydrogel alone, which cannot be easily adapted to the cartilage defect sites. Moreover, the SF-GMA/LKP composite scaffold could respond instantaneously, fill the cartilage defect site *in situ*, and promote the regenerative repair of cartilage. Surprisingly, the SF-GMA/LKP10 and SF-GMA/LKP20 composite hydrogel scaffolds provided optimal neocartilage. Our study provides a new therapeutic strategy for high-quality regenerative repair of cartilage defects.

CRediT authorship contribution statement

Deguang Wu: Conceptualization, Data curation, Formal analysis, Investigation, Methodology, Project administration, Resources, Software, Supervision, Validation, Visualization, Writing – original draft, Writing – review & editing. **Jian Li:** Methodology, Project administration, Resources, Writing – review & editing. **Chengxinqiao Wang:** Methodology, Supervision, Validation, Writing – review & editing. **Zhiwen Su:** Data curation, Methodology, Validation. **Hao Su:**

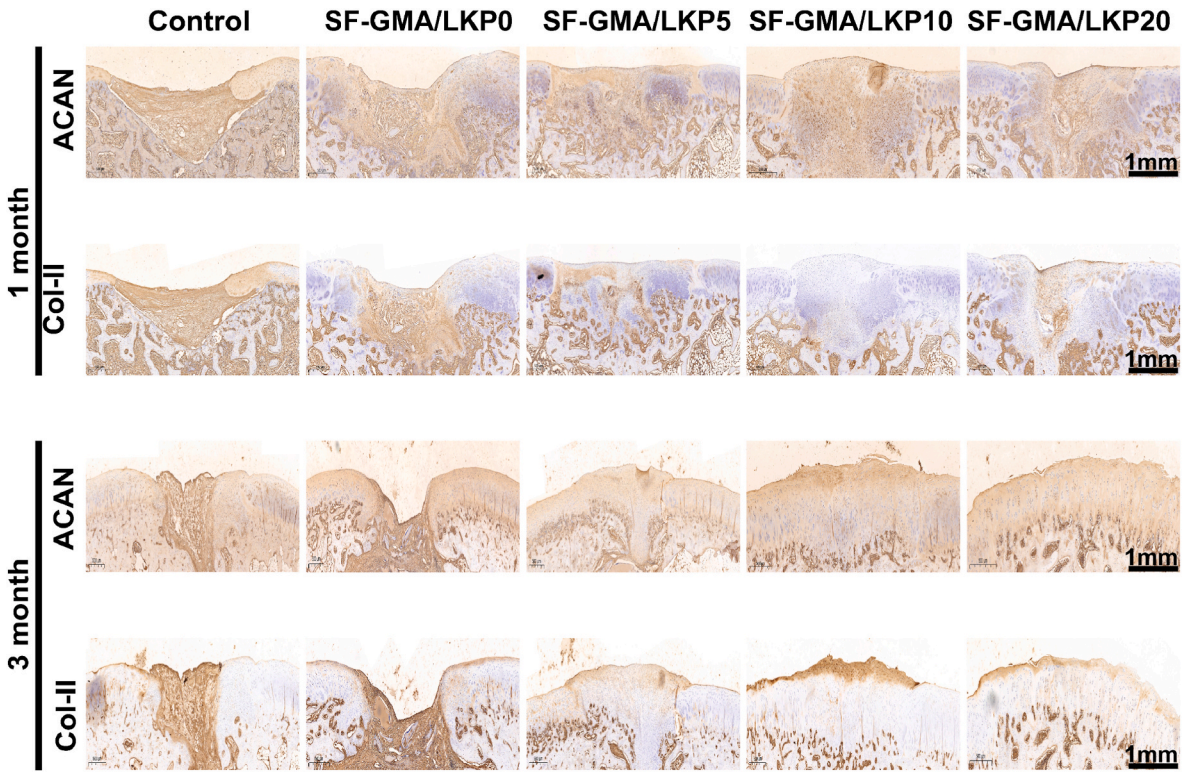

Fig. 12. Immunohistochemical staining of Col-II and ACAN in rabbit cartilage defects of 1 m and 3 m treated with different SF-GMA/LKP hydrogel scaffolds.

Methodology, Resources, Validation. **Yan Chen:** Conceptualization, Funding acquisition, Resources, Supervision, Writing – review & editing. **Bo Yu:** Conceptualization, Data curation, Formal analysis, Funding acquisition, Investigation, Methodology, Project administration, Resources, Software, Supervision, Validation, Visualization, Writing – original draft, Writing – review & editing.

Declaration of competing interest

The authors declare that they have no known competing financial interests or personal relationships that could have appeared to influence the work reported in this paper.

Data availability

Data will be made available on request.

Acknowledgments

This research was supported by multiple funding projects, including the National Natural Science Foundation of China (Grant Nos. 81974323 and 81871355), the Guangdong Basic and Applied Basic Research Foundation (Grant Nos. 2019A1515011638 and 2022A1515011292), the Natural Science Foundation of Guangdong Province of China (Grant No. 2018A030313078), and Science and Technology Projects in Guangzhou (Grant No. 202002030485).

Appendix A. Supplementary data

Supplementary data to this article can be found online at https://doi.org/10.1016/j.mtbio.2024.100962.

References

[1] Y.R. Chen, X. Yan, F.Z. Yuan, L. Lin, S.J. Wang, J. Ye, J.Y. Zhang, M. Yang, D. C. Wu, X. Wang, J.K. Yu, Kartogenin-conjugated double-network hydrogel combined with stem cell transplantation and tracing for cartilage repair, Adv. Sci. 9 (2022) e2105571, https://doi.org/10.1002/advs.202105571.

[2] X. Guo, Y. Ma, Y. Min, J. Sun, X. Shi, G. Gao, L. Sun, J. Wang, Progress and prospect of technical and regulatory challenges on tissue-engineered cartilage as therapeutic combination product, Bioact. Mater. 20 (2023) 501–518, https://doi.org/10.1016/j.bioactmat.2022.06.015.

[3] Y. Hua, H. Xia, L. Jia, J. Zhao, D. Zhao, X. Yan, Y. Zhang, S. Tang, G. Zhou, L. Zhu, Q. Lin, Ultrafast, tough, and adhesive hydrogel based on hybrid photocrosslinking for articular cartilage repair in water-filled arthroscopy, Sci. Adv. 7 (2021), https://doi.org/10.1126/sciadv.abg0628.

[4] K.N. Bailey, J. Nguyen, C.S. Yee, N.S. Dole, A. Dang, T. Alliston, Mechanosensitive control of articular cartilage and subchondral bone homeostasis in mice requires osteocytic transforming growth factor beta signaling, Arthritis Rheumatol. 73 (2021) 414–425, https://doi.org/10.1002/art.41548.

[5] J. Ying, P. Wang, S. Zhang, T. Xu, L. Zhang, R. Dong, S. Xu, P. Tong, C. Wu, H. Jin, Transforming growth factor-beta1 promotes articular cartilage repair through canonical smad and hippo pathways in bone mesenchymal stem cells, Life Sci. 192 (2018) 84–90, https://doi.org/10.1016/j.lfs.2017.11.028.

[6] H.L. Lee, B. Yu, P. Deng, C.Y. Wang, C. Hong, Transforming growth factor-beta-induced kdm4b promotes chondrogenic differentiation of human mesenchymal stem cells, Stem Cell. 34 (2016) 711–719, https://doi.org/10.1002/stem.2231.

[7] S. Qin, J. Zhu, G. Zhang, Q. Sui, Y. Niu, W. Ye, G. Ma, H. Liu, Research progress of functional motifs based on growth factors in cartilage tissue engineering: a review, Front. Bioeng. Biotechnol. 11 (2023), https://doi.org/10.3389/fbioe.2023.1127949.

[8] A.L. Caballero, S.M. Silva, S.E. Moulton, Growth factor delivery: defining the next generation platforms for tissue engineering, J. Contr. Release 306 (2019) 40–58, https://doi.org/10.1016/j.jconrel.2019.05.028.

[9] L. Oliver-Cervello, H. Martin-Gomez, L. Reyes, F. Noureddine, C.E. Ada, M. P. Ginebra, C. Mas-Moruno, An engineered biomimetic peptide regulates cell behavior by synergistic integrin and growth factor signaling, Adv. Healthcare Mater. 10 (2021) e2001757, https://doi.org/10.1002/adhm.202001757.

[10] S. Basu, M. Kumar, J.P. Chansuria, T.B. Singh, R. Bhatnagar, V.K. Shukla, Effect of cytomodulin-10 (tgf-beta1 analogue) on wound healing by primary intention in a murine model, Int. J. Surg. 7 (2009) 460–465, https://doi.org/10.1016/j.ijsu.2009.07.005.

[11] J.K. Sahoo, O. Hasturk, T. Falcucci, D.L. Kaplan, Silk chemistry and biomedical material designs, Nat. Rev. Chem 7 (2023) 302–318, https://doi.org/10.1038/s41570-023-00486-x.

[12] Y. Zhang, R. Sheng, J. Chen, H. Wang, Y. Zhu, Z. Cao, X. Zhao, Z. Wang, C. Liu, Z. Chen, P. Zhang, B. Kuang, H. Zheng, C. Shen, Q. Yao, W. Zhang, Silk fibroin and sericin differentially potentiate the paracrine and regenerative functions of stem cells through multiomics analysis, Adv. Mater. 35 (2023) e2210517, https://doi.org/10.1002/adma.202210517.

[13] X. Ding, W. Zhang, P. Xu, W. Feng, X. Tang, X. Yang, L. Wang, L. Li, Y. Huang, J. Ji, D. Chen, H. Liu, Y. Fan, The regulatory effect of braided silk fiber skeletons with

differential porosities on in vivo vascular tissue regeneration and long-term patency, Research 2022 (2022) 9825237, https://doi.org/10.34133/2022/9825237.
[14] Q. Li, W. Hu, Q. Huang, J. Yang, B. Li, K. Ma, Q. Wei, Y. Wang, J. Su, M. Sun, S. Cui, R. Yang, H. Li, X. Fu, C. Zhang, Mir146a-loaded engineered exosomes released from silk fibroin patch promote diabetic wound healing by targeting irak1, Signal Transduct. Targeted Ther. 8 2023 62. https://doi.org/10.1038/s41392-022-01263-w..
[15] M. Gholipourmalekabadi, S. Sapru, A. Samadikuchaksaraei, R.L. Reis, D.L. Kaplan, S.C. Kundu, Silk fibroin for skin injury repair: where do things stand? Adv. Drug Deliv. Rev. 153 (2020) 28–53, https://doi.org/10.1016/j.addr.2019.09.003.
[16] H.Y. Wang, Y.Q. Zhang, Z.G. Wei, Dissolution and processing of silk fibroin for materials science, Crit. Rev. Biotechnol. 41 (2021) 406–424, https://doi.org/10.1080/07388551.2020.1853030.
[17] I.P. Moreira, C. Esteves, S. Palma, E. Ramou, A. Carvalho, A. Roque, Synergy between silk fibroin and ionic liquids for active gas-sensing materials, Mater. Today Bio. 15 (2022) 100290, https://doi.org/10.1016/j.mtbio.2022.100290.
[18] H.Y. Wang, Y.Q. Zhang, Z.G. Wei, Excess acetone extraction in silk protein solution greatly accelerates the regeneration progress of silk fibroin for desalting and purification, Int. J. Biol. Macromol. 146 (2020) 588–595, https://doi.org/10.1016/j.ijbiomac.2019.12.274.
[19] H. Kgomo, S. Ncube, V. Mhuka, T.G. Kebede, S. Dube, M.M. Nindi, A comparative study on the dissolution of argema mimosae silk fibroin and fabrication of films and nanofibers, Polymers 13 (2021), https://doi.org/10.3390/polym13040549.
[20] H. Hong, Y.B. Seo, D.Y. Kim, J.S. Lee, Y.J. Lee, H. Lee, O. Ajiteru, M.T. Sultan, O. J. Lee, S.H. Kim, C.H. Park, Digital light processing 3d printed silk fibroin hydrogel for cartilage tissue engineering, Biomaterials 232 (2020) 119679, https://doi.org/10.1016/j.biomaterials.2019.119679.
[21] S.H. Kim, H. Hong, O. Ajiteru, M.T. Sultan, Y.J. Lee, J.S. Lee, O.J. Lee, H. Lee, H. S. Park, K.Y. Choi, J.S. Lee, H.W. Ju, I.S. Hong, C.H. Park, 3d bioprinted silk fibroin hydrogels for tissue engineering, Nat. Protoc. 16 (2021) 5484–5532, https://doi.org/10.1038/s41596-021-00622-1.
[22] F. Feng, X. Song, Z. Tan, Y. Tu, L. Xiao, P. Xie, Y. Ma, X. Sun, J. Ma, L. Rong, L. He, Cooperative assembly of a designer peptide and silk fibroin into hybrid nanofiber gels for neural regeneration after spinal cord injury, Sci. Adv. 9 (2023) eadg234, https://doi.org/10.1126/sciadv.adg0234.
[23] B. Cheng, Y. Yan, J. Qi, L. Deng, Z. Shao, K. Zhang, B. Li, Z. Sun, X. Li, Cooperative assembly of a peptide gelator and silk fibroin afford an injectable hydrogel for tissue engineering, ACS Appl. Mater. Interfaces 10 (2018) 12474–12484, https://doi.org/10.1021/acsami.8b01725.
[24] K. Wang, J.D. Keasling, S.J. Muller, Effects of the sequence and size of non-polar residues on self-assembly of amphiphilic peptides, Int. J. Biol. Macromol. 36 (2005) 232–240, https://doi.org/10.1016/j.ijbiomac.2005.06.006.
[25] N.R. Lee, C.J. Bowerman, B.L. Nilsson, Effects of varied sequence pattern on the self-assembly of amphipathic peptides, Biomacromolecules 14 (2013) 3267–3277, https://doi.org/10.1021/bm400876s.
[26] J. Lou, D.J. Mooney, Chemical strategies to engineer hydrogels for cell culture, Nat. Rev. Chem 6 (2022) 726–744, https://doi.org/10.1038/s41570-022-00420-7.
[27] P. Aprile, I.T. Whelan, B.N. Sathy, S.F. Carroll, D.J. Kelly, Soft hydrogel environments that facilitate cell spreading and aggregation preferentially support chondrogenesis of adult stem cells, Macromol. Biosci. 22 (2022) e2100365, https://doi.org/10.1002/mabi.202100365.
[28] P. Kangari, T. Talaei-Khozani, I. Razeghian-Jahromi, M. Razmkhah, Mesenchymal stem cells: amazing remedies for bone and cartilage defects, Stem Cell Res. Ther. 11 (2020) 492, https://doi.org/10.1186/s13287-020-02001-1.
[29] J.A. Panadero, S. Lanceros-Mendez, J.L. Ribelles, Differentiation of mesenchymal stem cells for cartilage tissue engineering: individual and synergetic effects of three-dimensional environment and mechanical loading, Acta Biomater. 33 (2016) 1–12, https://doi.org/10.1016/j.actbio.2016.01.037.
[30] K. Zha, Z. Sun, Y. Yang, M. Chen, C. Gao, L. Fu, H. Li, X. Sui, Q. Guo, S. Liu, Recent developed strategies for enhancing chondrogenic differentiation of msc: impact on msc-based therapy for cartilage regeneration, Stem Cell. Int. 2021 (2021) 8830834, https://doi.org/10.1155/2021/8830834.
[31] Y. Hua, Y. Huo, B. Bai, J. Hao, G. Hu, Z. Ci, X. Wu, M. Yu, X. Wang, H. Chen, W. Ren, Y. Zhang, X. Wang, G. Zhou, Fabrication of biphasic cartilage-bone integrated scaffolds based on tissue-specific photo-crosslinkable acellular matrix hydrogels, Mater. Today Bio. 17 (2022) 100489, https://doi.org/10.1016/j.mtbio.2022.100489.
[32] C. Levinson, M. Lee, L.A. Applegate, M. Zenobi-Wong, An injectable heparin-conjugated hyaluronan scaffold for local delivery of transforming growth factor beta1 promotes successful chondrogenesis, Acta Biomater. 99 (2019) 168–180, https://doi.org/10.1016/j.actbio.2019.09.017.
[33] X. Ding, J. Gao, X. Yu, J. Shi, J. Chen, L. Yu, S. Chen, J. Ding, 3d-printed porous scaffolds of hydrogels modified with tgf-beta1 binding peptides to promote in vivo cartilage regeneration and animal gait restoration, ACS Appl. Mater. Interfaces 14 (2022) 15982–15995, https://doi.org/10.1021/acsami.2c00761.
[34] W. Wei, H. Dai, Articular cartilage and osteochondral tissue engineering techniques: recent advances and challenges, Bioact. Mater. 6 (2021) 4830–4855, https://doi.org/10.1016/j.bioactmat.2021.05.011.
[35] C. Lesage, M. Lafont, P. Guihard, P. Weiss, J. Guicheux, V. Delplace, Material-assisted strategies for osteochondral defect repair, Adv. Sci. 9 (2022) e2200050, https://doi.org/10.1002/advs.202200050.
[36] L. Yu, S. Cavelier, B. Hannon, M. Wei, Recent development in multizonal scaffolds for osteochondral regeneration, Bioact. Mater. 25 (2023) 122–159, https://doi.org/10.1016/j.bioactmat.2023.01.012.